

# The Magellanic Edges Survey – IV. Complex tidal debris in the SMC outskirts

L. R. Cullinane<sup>1,2\*</sup>, A. D. Mackey<sup>2</sup>, G. S. Da Costa<sup>2</sup>, S. E. Koposov<sup>3,4</sup>, D. Erkal<sup>5</sup>

<sup>1</sup>*Department of Physics and Astronomy, Johns Hopkins University, Baltimore, MD 21218, USA*

<sup>2</sup>*Research School of Astronomy and Astrophysics, Australian National University, Canberra, ACT 2611, Australia*

<sup>3</sup>*Institute for Astronomy, University of Edinburgh, Royal Observatory, Blackford Hill, Edinburgh EH9 3HJ, UK*

<sup>4</sup>*Institute of Astronomy, University of Cambridge, Madingley Road, Cambridge CB3 0HA, UK*

<sup>5</sup>*Department of Physics, University of Surrey, Guildford GU2 7XH, UK*

Accepted XXX. Received YYY; in original form ZZZ

## ABSTRACT

We use data from the Magellanic Edges Survey (MagES) in combination with Gaia EDR3 to study the extreme southern outskirts of the Small Magellanic Cloud (SMC), focussing on a field at the eastern end of a long arm-like structure which wraps around the southern periphery of the Large Magellanic Cloud (LMC). Unlike the remainder of this structure, which is thought to be comprised of perturbed LMC disk material, the aggregate properties of the field indicate a clear connection with the SMC. We find evidence for two stellar populations in the field: one having properties consistent with the outskirts of the main SMC body, and the other significantly perturbed. The perturbed population is on average  $\sim 0.2$  dex more metal-rich, and is located  $\sim 7$  kpc in front of the dominant population with a total space velocity relative to the SMC centre of  $\sim 230$  km s<sup>-1</sup> broadly in the direction of the LMC. We speculate on possible origins for this perturbed population, the most plausible of which is that it comprises debris from the inner SMC that has been recently tidally stripped by interactions with the LMC.

**Key words:** Magellanic Clouds – galaxies: kinematics and dynamics – galaxies: structure

## 1 INTRODUCTION

The Large and Small Magellanic Clouds (LMC/SMC) are exemplary testbeds for studying the effects of tidal interactions on galaxy evolution. Dynamical models suggest the Clouds have likely repeatedly interacted with each other over several Gyr (e.g. Besla et al. 2012; Pardy et al. 2018; Cullinane et al. 2022). The infall of the Clouds into the Milky Way gravitational potential has also influenced the system (e.g. Cullinane et al. 2021; Lucchini et al. 2021). Each of these interactions leaves imprints on the star formation, structure, and kinematics of the Clouds, and at distances of  $\sim 50$  kpc and  $\sim 60$  kpc for the LMC and SMC respectively (Pietrzyński et al. 2019; Graczyk et al. 2020), these signatures can be studied in detail to precisely constrain the history of the Magellanic system.

As the smaller Magellanic galaxy, the SMC is particularly susceptible to perturbation through interactions with both the LMC and Milky Way. It is significantly extended along the line of sight (LOS), with depths of up to 20–30 kpc, particularly in its eastern regions (e.g. Hatzidimitriou & Hawkins 1989; Nidever et al. 2013; Scowcroft et al. 2016; Subramanian et al. 2017; El Yousoufi et al. 2021). Deep photometric studies (e.g. Cioni et al. 2011; Nidever et al. 2017), in addition to data from the Gaia satellite (Gaia Collaboration et al. 2018, 2021), have also revealed numerous extended stellar substructures surrounding the SMC (e.g. Pieres et al. 2017; Mackey et al. 2018; Belokurov & Erkal 2019; Massana et al. 2020). Full kinematic data are crucial in understanding the origins of these features, and

by extension, the interaction history of the Clouds. Analysis of an eastern SMC foreground population (Omkumar et al. 2020; James et al. 2021) find it has motion distinct from the SMC body, and suggest it may have formed via tidal stripping of the SMC during its last pericentric passage around the LMC  $\sim 150$  Myr ago (Zivick et al. 2018). Studies of the inner ( $\lesssim 6^\circ$ ) SMC using 3D stellar kinematics (De Leo et al. 2020; Zivick et al. 2021) reveal it is being torn apart, likely also due to this recent pericentric passage. However, LOS velocity information is scarce in the extreme SMC outskirts.

The Magellanic Edges Survey (MagES; Cullinane et al. 2020, hereafter Paper I) is designed to fill this gap. MagES is a spectroscopic survey using the 2dF+AAOmega instrument on the Anglo-Australian Telescope (Lewis et al. 2002; Sharp & Birchall 2010), providing LOS velocities and select abundance data for red clump (RC) and red giant branch (RGB) stars across the Magellanic periphery. In combination with astrometry from Gaia EDR3, it allows for the derivation of the 3D kinematics necessary to constrain Magellanic interactions.

In this Letter, we present a detailed study of MagES field 3, located in the SMC outskirts near the end of a long arm-like structure south of the LMC. In the third MagES paper (Cullinane et al. 2022, hereafter Paper III), we suggested this field appears associated with the SMC; however, further analysis suggests it may contain two kinematically distinct populations. Intriguingly, despite its close proximity to other Magellanic structures – including the likely-LMC-associated arm, mixed LMC-SMC debris (Cheng et al. 2022), and SMC foreground populations (e.g. James et al. 2021) – the characteristics of this field are unique. Here, we explore the properties of this field using full 3D kinematics, and suggest potential origins for the material within it.

\* E-mail: lcullin4@jhu.edu (LRC)

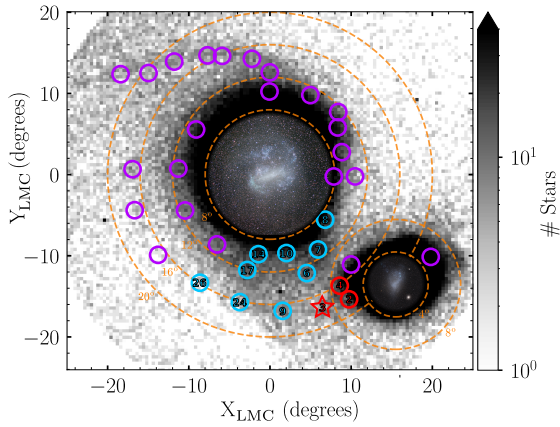


**Figure 1.** Location of MagES fields across the Magellanic periphery. The three SMC fields discussed in this letter are red, with field 3 starred. Reference fields in the outer LMC are blue, and fields not discussed here are purple. The background image shows the density of Magellanic red clump/RGB stars per square degree, selected from Gaia EDR3 as in Paper III. ( $X_{\text{LMC}}, Y_{\text{LMC}}$ ) are coordinates in an orthographic projection centred on the LMC; north is up and east is to the left. Orange dashed circles mark angular separations of  $8^\circ/12^\circ/16^\circ/20^\circ$  from the LMC centre, and  $4^\circ/8^\circ$  from the SMC centre.

## 2 DATA

In addition to field 3, this letter discusses fields 2 and 4, which lie in the nearby southern SMC outskirts and are used as control fields. Field locations are shown in Fig. 1. Readers are referred to Papers I and III for a detailed description of the survey. We use the statistical framework described in Paper I to probabilistically associate stars to either the Clouds, or one of several possible Milky Way contaminant populations, based on their kinematics. We typically use a single multi-dimensional Gaussian distribution – characterised by the aggregate LOS velocity ( $V_{\text{LOS}}$ ), proper motions ( $\mu_\alpha, \mu_\delta$ )<sup>1</sup>, and associated dispersions ( $\sigma_{\text{LOS}}, \sigma_\alpha, \sigma_\delta$ ) – to describe the Magellanic population in a field. Nevertheless, our framework allows for additional components to be included (see §4). Table 1 provides the location, inferred kinematic and photometric properties, and number of stars with probabilities  $\geq 50\%$  of being associated with the Clouds, for each field discussed in this Letter.

For sufficiently bright ( $G > 18$ ) RGB stars<sup>2</sup>, MagES estimates [Fe/H] using the equivalent width of CaII triplet lines (see Paper I). For fainter red clump stars, we stack spectra for likely ( $P_i \geq 50\%$ ) Magellanic stars to create a single “representative” spectrum used for these measurements; the resulting [Fe/H] estimates tend towards the mean metallicity of the given field. The mean red clump magnitude at the location of each field, used in this process, is calculated as in Paper III. All metallicity estimates have uncertainties of 0.2 dex.

## 3 AGGREGATE PROPERTIES

Based on its location, field 3 could plausibly contain debris from both Clouds. Consequently, to obtain an initial estimate of the field’s composition, we compare its aggregate properties to those of nearby MagES fields comprised predominantly of material from only the LMC or SMC. The top panel of Fig. 2 presents the aggregate proper motions, colour-coded by the aggregate LOS velocity, for field 3

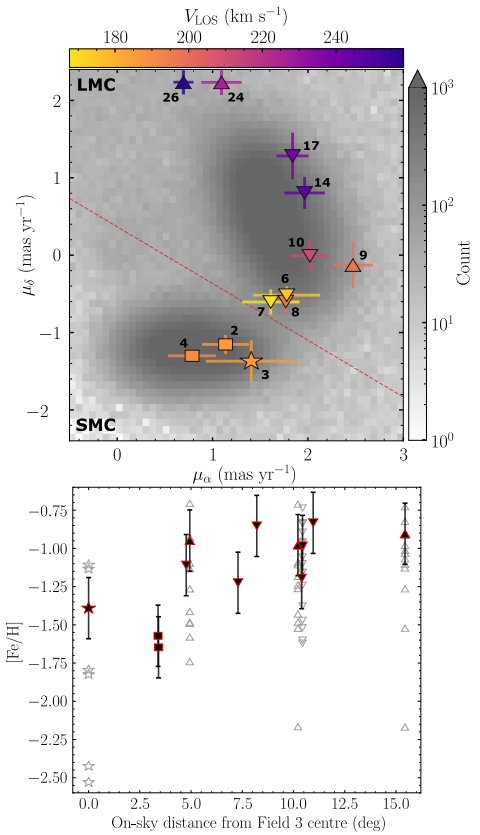


**Figure 2.** *Top:* Aggregate proper motions for MagES fields, colour-coded by their aggregate LOS velocity. Symbols denote field 3 (starred point), fields 2/4 in the SMC outskirts (square points), LMC fields from Paper III along the southern arm-like structure (upwards-pointing triangles), and LMC southern disk and claw fields (downwards-pointing triangles, also from Paper III). These are overlaid on a 2D density plot of Gaia EDR3 proper motions for likely-Magellanic RC stars, selected as in §3. The red dashed line shows an approximate boundary between LMC-like (upper right) and SMC-like (lower left) proper motions. *Bottom:* [Fe/H] estimates for MagES fields as a function of on-sky distance from field 3, with symbols as in the top panel. Solid points represent results from stacked spectra, which approximate the mean metallicity of the field. Open points represent [Fe/H] estimates for individual bright ( $G > 18$ ) RGB stars within fields where these are observed; associated uncertainties are omitted for clarity.

(starred point), fields 2 and 4 in the SMC outskirts, and several fields across the southern LMC outskirts from Paper III. These are overlaid on a density plot of likely Magellanic RC stars selected from Gaia EDR3, with galactocentric radii  $6^\circ < R_{\text{LMC}} < 20^\circ$  and  $2^\circ < R_{\text{SMC}} < 10^\circ$ . For this sample, we utilise the CMD selection box described in §2.4 of Paper III, imposing quality cuts  $r_{\text{WE}} < 1.4$  and  $|C^*| < 3\sigma_{C^*}$ , a parallax cut  $\varpi < 0.15$  mas, and proper motion cuts  $0.4 < \mu_\alpha (\text{mas yr}^{-1}) < 2.5$ ,  $-1.6 < \mu_\delta (\text{mas yr}^{-1}) < 2.5$ . The red dashed line marks an approximate boundary between LMC-like (upper right) and SMC-like (lower left) proper motions. The bottom panel of Fig. 2 presents [Fe/H] measurements for the same fields as a function of on-sky distance from the centre of field 3.

Fields 2 and 4 (square points in Fig. 2) are clearly distinct from the LMC-associated reference fields. These fields sit firmly within the region of proper motion space associated with the SMC, and have mean metallicities  $\sim 0.5$  dex lower than fields dominated by LMC material: a difference broadly consistent with that expected given the relative masses of the Clouds. While the mean [Fe/H] values of these fields ( $\sim -1.6$ ) are lower than literature metallicity

<sup>1</sup> where  $\mu_\alpha$  includes the usual  $\cos(\delta)$  correction.

<sup>2</sup> with six observed in field 3, but none in fields 2 and 4.

**Table 1.** Properties for MagES fields analysed in this paper. Columns give the field centre position (RA, DEC in J2000.0); number of likely ( $P_i \geq 50\%$ ) Magellanic stars ( $N_{\text{Mag}}$ ); on-sky SMC and LMC galactocentric radii ( $R_{\text{SMC}}/R_{\text{LMC}}$ ); aggregate kinematic and photometric properties; and the field mean [Fe/H] with uncertainty 0.2 dex. All properties are calculated as described in §2: we report the 68% confidence interval as the  $1\sigma$  uncertainty in each parameter.

Field	RA ( $\alpha$ )	DEC ( $\delta$ )	$N_{\text{Mag}}$	$R_{\text{SMC}}$ (deg)	$R_{\text{LMC}}$ (deg)	$V_{\text{LOS}}$ ( $\text{km s}^{-1}$ )	$\sigma_{\text{LOS}}$ ( $\text{km s}^{-1}$ )	$\mu_{\alpha}$ ( $\text{mas yr}^{-1}$ )	$\sigma_{\alpha}$ ( $\text{mas yr}^{-1}$ )	$\mu_{\delta}$ ( $\text{mas yr}^{-1}$ )	$\sigma_{\delta}$ ( $\text{mas yr}^{-1}$ )	$\langle (BP-RP)_0 \rangle$	$\sigma_{(BP-RP)_0}$	$\langle G_0 \rangle$	$\sigma_{G_0}$	[Fe/H]
2	00 59 30.00	-79 10 57.00	152	6.05	18.87	189.9 $\pm$ 2.9	34.3 $\pm$ 2.2	0.79 $\pm$ 0.03	0.25 $\pm$ 0.03	-1.30 $\pm$ 0.02	0.06 $\pm$ 0.03	0.91 $\pm$ 0.03	0.13 $\pm$ 0.05	19.00 $\pm$ 0.05	0.28 $\pm$ 0.07	-1.6
4	01 45 11.00	-79 15 22.00	152	6.86	16.74	185.5 $\pm$ 2.2	24.2 $\pm$ 1.8	1.14 $\pm$ 0.03	0.25 $\pm$ 0.03	-1.15 $\pm$ 0.02	0.12 $\pm$ 0.03	0.92 $\pm$ 0.02	0.09 $\pm$ 0.02	18.96 $\pm$ 0.03	0.20 $\pm$ 0.06	-1.6
3	01 20 00.00	-82 30 00.00	68	9.45	18.07	185.4 $\pm$ 4.1	31.4 $\pm$ 3.2	1.41 $\pm$ 0.07	0.48 $\pm$ 0.05	-1.37 $\pm$ 0.04	0.27 $\pm$ 0.05	0.93 $\pm$ 0.03	0.11 $\pm$ 0.06	18.77 $\pm$ 0.07	0.31 $\pm$ 0.06	-1.4

measurements at smaller SMC radii ( $\sim 1$ : e.g. Dobbie et al. 2014), they do approximately follow the negative radial metallicity gradient in the SMC (e.g. Cioni 2009; Dobbie et al. 2014), and also agree with photometric metallicity estimates in this region (Grady et al. 2021). We thus conclude that these fields are dominated by SMC material.

Kinematically, field 3 is most similar to fields 2 and 4, with proper motions and a LOS velocity consistent with those of the SMC body. With a mean [Fe/H]  $\sim -1.4$ , field 3 is mildly more metal-rich than the nearby SMC fields (though still consistent within uncertainty), but somewhat more metal-poor than the average metallicity ([Fe/H]  $\sim -1$ ) of the nearby LMC-dominated fields. This may indicate a mix of LMC and SMC material in the field; however, it is also consistent with expectations for stars originating in more central SMC regions.

## 4 TWO DISTINCT SMC POPULATIONS?

The preceding analysis assumes field 3 is comprised of a single population of stars. However, inspection of the LOS velocity and proper motion distributions of likely Magellanic members<sup>3</sup> in the field, as in Fig. 3, suggests the situation may be more complicated. Unlike other MagES fields, which have clear unimodal velocity distributions (Paper I; Paper III), the  $\mu_{\alpha}$  distribution and, at lower significance, the LOS velocity distribution in field 3 both appear bimodal. Fig. 3 thus hints at field 3 containing two populations of stars with distinct kinematics, highlighted by the dashed selection boxes. One set – comprising  $\sim 65\%$  of the Magellanic stars in the field – is broadly consistent with the kinematics of the nearby SMC body<sup>4</sup>, with total proper motion  $\sqrt{\mu_{\alpha}^2 + \mu_{\delta}^2} \sim 1.6 \text{ mas yr}^{-1}$ , and a median LOS velocity  $\sim 195 \text{ km s}^{-1}$ . We henceforth refer to these stars as the “bulk” population. The putative second population has a larger total proper motion ( $\sim 2.6 \text{ mas yr}^{-1}$ ), but a lower median LOS velocity ( $\sim 160 \text{ km s}^{-1}$ ); we henceforth refer to these stars as the “offset” population.

We test fitting these two potential populations using separate Gaussian distributions in addition to the MW foreground as in §2. Comparing this with the single-component fit using the Bayesian Information Criterion (Schwarz 1978) shows there is insufficient evidence to prefer the two-component fit. However, in the restricted case of one- and two-component fits to only likely Magellanic members, we find the two-component fit is preferred. The relatively low number of stars in both populations and the moderate kinematic uncertainties for each individual star likely both contribute to the single-population solution being preferred when the background is included.

Nonetheless, as the possibility of two populations is intriguing, we proceed with an investigation into the properties of the two groups of stars as defined in Fig. 3. For stars with Magellanic probability

<sup>3</sup> i.e. with aggregate probabilities  $\geq 50\%$  of being associated with the Clouds according to the single-component fit described in §2; all probabilities quoted subsequently are also based on this fit.

<sup>4</sup> While the systemic SMC LOS velocity is  $\sim 150 \text{ km s}^{-1}$ , the observed LOS velocity increases in a direction roughly towards field 3 due to the SMC’s disruption by the LMC (De Leo et al. 2020).

$\geq 50\%$  within each selection box, we present median 3D kinematics and dispersions (calculated as the standard deviation), in Table 2. Associated uncertainties are determined via bootstrapping. These measurements confirm the kinematic differences between the bulk and offset populations indicated by the histograms in Fig. 3; varying the selection box limits does not change this conclusion.

We additionally determine mean metallicity estimates for the two groups by stacking likely Magellanic RC star spectra as in §2. This shows that the offset population is  $\sim 0.2$  dex more metal-rich than the bulk population. Photometric differences are also possible, but unfortunately there are insufficient likely Magellanic stars in each selection box to fit photometric RC properties using the methods described in Paper III. Consequently, we expand our selection for this calculation only, taking stars from the Gaia sample described in §3, within the selection boxes in Fig. 3, with on-sky radii  $\leq 1.5^\circ$  from field 3. Table 2 presents the resulting  $G_0$  magnitude,  $(G_{\text{BP}} - G_{\text{RP}})_0$  colour, and associated dispersions for the two groups, taking the 68% confidence interval on these values as the associated uncertainty, and the right panel of Fig. 3 presents a Hess diagram for the stars.

These measurements show the offset population is mildly redder than the bulk population, likely a result of its  $\sim 0.2$  dex higher metallicity: in optical bands, metal-rich RC stars are intrinsically fainter and redder than those that are metal-poor (Girardi & Salaris 2001). To quantify this, we use PARSEC isochrones (Bressan et al. 2012)<sup>5</sup> to test the predicted photometry variations in Gaia EDR3 passbands for the metallicities of the two populations. The isochrones, for an 11 Gyr population assuming default IMF parameters, predict that the measured metallicity difference results in colour variations of  $\sim 0.05$  mag, consistent with that observed. While age can also affect the photometric properties of the red clump (e.g. Girardi & Salaris 2001), the lack of younger ( $\leq 4$  Gyr) main sequence stars above an ancient ( $\sim 11$  Gyr) turnoff in deep DECam photometry of the field (Mackey et al. 2018) implies a similar lack of young RC stars.

The offset population is also  $\sim 0.25$  mag brighter than the bulk population. However this cannot be due to the difference in metallicity, as the more metal-rich offset population is nominally intrinsically fainter by  $\sim 0.02$  mag. This suggests the offset population is located substantially in front of the bulk population. A back-of-the-envelope calculation assuming the observed magnitude difference between the two populations is due entirely to distance effects, and that the bulk population has a distance of 60 kpc<sup>6</sup>, implies the offset population is located  $\sim 7 \pm 2$  kpc in front of the bulk population.

## 5 DISCUSSION

The fact that splitting the Magellanic members in field 3 according to  $\mu_{\alpha}$  leads to clear splits in metallicity, LOS velocity, and LOS distance, strongly supports the idea that two distinct populations are

<sup>5</sup> Accessed as version 3.4 at <http://stev.oapd.inaf.it/cmd>.

<sup>6</sup> The measured  $\langle G_0 \rangle$  for the bulk population is broadly consistent with isochrone predictions for a similar stellar population at this distance.

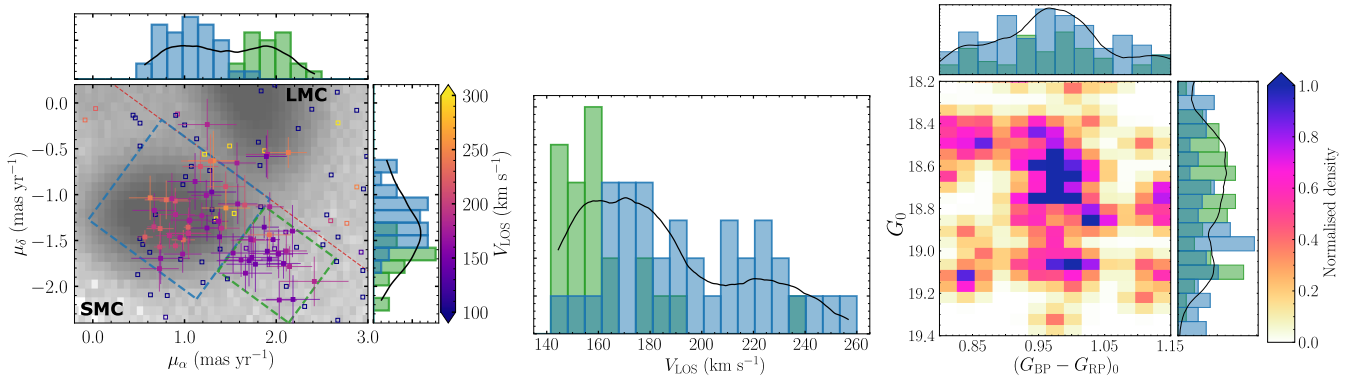


**Figure 3.** *Left:* Proper motion distribution of stars within field 3, colour-coded by their LOS velocity. Stars with probabilities <50% of being associated with the Clouds based on fitting a single Magellanic population are represented as hollow points without associated uncertainties. The background image is as per Fig. 2. Dashed lines indicate selection boxes used to define two subgroups in the field; the “bulk” population most consistent with the SMC body (blue), and the “offset” population (green). Top and side panels show proper motion histograms for the two subgroups (including only likely Magellanic members). Smooth curves overlaid in black are derived via kernel density estimation using an Epanechnikov kernel with bandwidth optimised using grid search cross-validation for all likely Magellanic stars. *Centre:* LOS velocity histogram for the two subgroups. *Right:* Hess diagram for stars within  $1.5^\circ$  of field 3, selected from Gaia as described below. Top and side panels show associated color and magnitude histograms for the two subgroups.

**Table 2.** Properties of two subgroups of stars in field 3, discussed in §4. Kinematic properties are calculated using MagES stars with probabilities  $\geq 50\%$  of being associated with the Clouds, and photometric properties are calculated using Gaia-selected RC stars with on-sky radii  $\leq 1.5^\circ$  from the field centre as in §3.

Group	$N_{\text{Mag}}$	$V_{\text{LOS}}$ ( $\text{km s}^{-1}$ )	$\sigma_{\text{LOS}}$ ( $\text{km s}^{-1}$ )	$\mu_\alpha$ ( $\text{mas yr}^{-1}$ )	$\sigma_\alpha$ ( $\text{mas yr}^{-1}$ )	$\mu_\delta$ ( $\text{mas yr}^{-1}$ )	$\sigma_\delta$ ( $\text{mas yr}^{-1}$ )	$\langle (BP - RP)_0 \rangle$	$\sigma_{(BP-RP)_0}$	$\langle G_0 \rangle$	$\sigma_{G_0}$	[Fe/H]
Bulk	37	$195.2 \pm 7.5$	$27.9 \pm 4.0$	$1.05 \pm 0.08$	$0.28 \pm 0.04$	$-1.25 \pm 0.08$	$0.28 \pm 0.05$	$0.92 \pm 0.04$	$0.10 \pm 0.05$	$19.00 \pm 0.06$	$0.19 \pm 0.08$	-1.4
Offset	22	$162.3 \pm 7.1$	$19.7 \pm 8.5$	$1.92 \pm 0.08$	$0.21 \pm 0.05$	$-1.68 \pm 0.07$	$0.20 \pm 0.05$	$0.98 \pm 0.01$	$0.04 \pm 0.02$	$18.74 \pm 0.07$	$0.24 \pm 0.06$	-1.2

present. We can make several inferences regarding possible origins of this material based on the properties of these populations.

Given the similarity between the kinematic and photometric properties of the bulk population and the two nearby MagES SMC fields (see Table 2), it seems likely that these stars comprise material from the local outskirts of the SMC. Further, models of debris produced in the SMC’s recent disruption by the LMC in Belokurov et al. (2017) have similar kinematics to the bulk population in the vicinity of field 3, supporting this hypothesis. The origin of the offset population is, however, less clear; no material with similar kinematic properties is observed in the Belokurov et al. (2017) models. It is important to emphasise that the properties of field 3 cannot simply be explained by a single population spread across a large line-of-sight depth. This is in contrast to dual red clump features observed throughout much of the SMC (e.g. Nidever et al. 2013; Subramanian et al. 2017; El Yousoufi et al. 2021), which do not show significant colour variations within individual fields, and which are well-described as the result of a distance spread much larger ( $>12$  kpc) than that observed here.

Although the offset population has some common characteristics with a foreground SMC substructure at galactocentric radii  $\lesssim 6^\circ$  (Omkar et al. 2020; James et al. 2021) – including larger proper motions, lower LOS velocities, and a closer distance than the main SMC body – they are sufficiently different that we suggest a direct connection is unlikely. In particular, the proper motions of that foreground substructure ( $\mu_\alpha, \mu_\delta \sim 1.1, -1.3$   $\text{mas yr}^{-1}$ ) are located entirely within our selection box for the bulk population. Further, the substructure is located  $\sim 13$  kpc in front of the main SMC population; nearly double the difference between the offset and bulk populations.

The comparatively high metallicity of the offset population relative to both the bulk population and nearby SMC fields indicates these stars are unlikely to be associated with the disrupted remains of an accreted Magellanic satellite. Since the offset population comprises only  $\sim 1/3$  of the likely Magellanic stars in field 3, this suggests any postulated disrupted satellite would have a low stellar mass, and

hence be more metal-poor than the SMC (Kirby et al. 2013).

Another possibility is that the offset population is comprised of LMC stars: either associated with an LMC halo, or originating in the far outskirts of the LMC disk and subsequently perturbed during tidal interactions. For example, Majewski et al. (2008) find a nominal LMC halo population having a similar mean metallicity ([Fe/H]  $\sim -1.2$ ) to the offset population in fields at similar galactocentric radii, but located on almost the diametric opposite side of the LMC from field 3. The mean metallicity and red clump colour of the offset population are also consistent within uncertainty with nearby LMC-disk-associated MagES fields (cf. Paper III), indicating they may be comprised of similar stellar populations. However, the offset population kinematics are significantly different than expected in these scenarios. The much lower LOS velocity of the offset population ( $\sim 160$   $\text{km s}^{-1}$ ) compared to the systemic velocity of the LMC ( $\sim 260$   $\text{km s}^{-1}$ : van der Marel & Kallivayalil 2014) is inconsistent with that predicted for either the LMC disk or halo at the position of field 3. The offset population also has a total space velocity relative to the LMC centre ( $\sim 140$   $\text{km s}^{-1}$ ) approximately double that of the most perturbed MagES LMC substructure fields (cf. Paper III), rendering an association with the LMC unlikely.

A more plausible origin is that the offset population comprises material originating at substantially smaller SMC radii, which has been perturbed and driven outwards. Given the mean metallicity in the inner SMC is approx.  $-1$  (e.g. Dobbie et al. 2014), the metallicity of the offset population ( $\sim -1.2$ ) is broadly consistent with this scenario. As seen in Fig. 4, which presents the projected velocities of the two populations relative to the SMC centre, the velocity of the offset population is broadly in the direction of the LMC – much more so than for the bulk population and nearby SMC fields. The large space velocity of the offset population ( $\sim 230$   $\text{km s}^{-1}$ ) naively implies a time of just over 50 Myr to cover the distance between the SMC centre and the position of field 3, suggesting the material may be recently perturbed. The SMC pericentric passage around the LMC  $\sim 150$  Myr

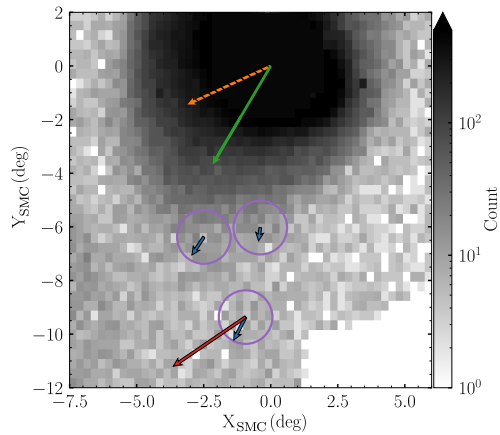


**Figure 4.** Projected proper motions for MagES fields (purple circles) in the SMC outskirts relative to the SMC centre. Blue arrows show motions for fields 2, 4, and the bulk population in field 3; the red arrow shows the motion of the offset population in field 3. The green arrow indicates the systemic proper motion of the SMC, with the dashed orange arrow indicating the direction of the LMC. The background image shows the stellar density for the same sample of Magellanic stars as in the top panel of Fig. 2. The orientation of this figure is rotated  $\sim 90^\circ$  clockwise relative to Fig. 1.

ago (Zivick et al. 2018), thought to be a near head-on collision at a distance  $\leq 10$  kpc from the LMC centre (Choi et al. 2022), thus seems a likely contender for the source of this perturbation.

We also note there are a few stars ( $<10$ ) in fields 2 and 4 with velocities within  $1\sigma$  of the median offset population kinematics, which may have similar origins. Unfortunately, there are too few such stars to reliably check the consistency of metallicity or photometric properties. Notably, however, there are no stars in the nearby LMC-associated fields with kinematics matching the offset group, adding weight to our hypothesis that this population is linked to the SMC.

In summary, we have discussed the complex kinematics of MagES field 3, located in the extreme southern outskirts of the SMC. While the aggregate properties of the field are consistent with an SMC origin, there are indications that two distinct sets of stars may be present: a “bulk” population with similar characteristics to the outskirts of the main SMC body, and an “offset” population with distinct photometric, kinematic, and chemical properties. We discuss several possible origins for this offset population, concluding that it is most plausibly comprised of debris from the inner SMC recently perturbed by the LMC. Our analysis illustrates the power of 3D kinematics in identifying structures otherwise invisible due to projection, and which – in conjunction with future detailed modelling – potentially hold great power for constraining the details of Magellanic interactions.

## ACKNOWLEDGEMENTS

This work has made use of data from the European Space Agency (ESA) mission *Gaia* (<https://www.cosmos.esa.int/gaia>), processed by the *Gaia* Data Processing and Analysis Consortium (DPAC, <https://www.cosmos.esa.int/web/gaia/dpac/consortium>). Funding for the DPAC has been provided by national institutions, in particular the institutions participating in the *Gaia* Multilateral Agreement. Based on data acquired at the Anglo-Australian Observatory. We acknowledge the traditional owners of the land on which the AAT stands, the Gamilaraay people, and pay our respects to elders past, present and emerging. LRC & ADM acknowledge support from an ARC Future Fellowship (FT160100206). For the purpose of open access, the author has applied a Creative

Commons Attribution (CC BY) licence to any Author Accepted Manuscript version arising from this submission.

## DATA AVAILABILITY

Underlying data will be shared on reasonable request to the authors.

## REFERENCES

- Belokurov V., Erkal D., 2019, *MNRAS*, 482, L9
- Belokurov V., Erkal D., Deason A. J., Koposov S. E., De Angeli F., Wyn Evans D., Fraternali F., Mackey D., 2017, *MNRAS*, 466, 4711
- Besla G., Kallivayalil N., Hernquist L., van der Marel R. P., Cox T. J., Kereš D., 2012, *MNRAS*, 421, 2109
- Bressan A., Marigo P., Girardi L., Salasnich B., Dal Cero C., Rubele S., Nanni A., 2012, *MNRAS*, 427, 127
- Cheng X., et al., 2022, *ApJ*, 928, 95
- Choi Y., Olsen K. A. G., Besla G., van der Marel R. P., Zivick P., Kallivayalil N., Nidever D. L., 2022, *ApJ*, 927, 153
- Cioni M.-R. L., 2009, *A&A*, 506, 1137
- Cioni M.-R., et al., 2011, *A&A*, 527, A116
- Cullinane L. R., et al., 2020, *MNRAS*, 497, 3055
- Cullinane L. R., Mackey A. D., Da Costa G. S., Erkal D., Koposov S. E., Belokurov V., 2021, *MNRAS*, 510, 445
- Cullinane L. R., Mackey A. D., Da Costa G. S., Erkal D., Koposov S. E., Belokurov V., 2022, *MNRAS*, 512, 4798
- De Leo M., Carrera R., Noël N. E. D., Read J. I., Erkal D., Gallart C., 2020, *MNRAS*, 495, 98
- Dobbie P. D., Cole A. A., Subramaniam A., Keller S., 2014, *MNRAS*, 442, 1680
- El Youssoufi D., et al., 2021, *MNRAS*, 505, 2020
- Gaia Collaboration et al., 2018, *A&A*, 616, A12
- Gaia Collaboration et al., 2021, *A&A*, 649, A1
- Girardi L., Salaris M., 2001, *MNRAS*, 323, 109
- Graczyk D., et al., 2020, *ApJ*, 904, 13
- Grady J., Belokurov V., Evans N. W., 2021, *ApJ*, 909, 150
- Hatzidimitriou D., Hawkins M. R. S., 1989, *MNRAS*, 241, 667
- James D., et al., 2021, *MNRAS*, 508, 5854
- Kirby E. N., Cohen J. G., Guhathakurta P., Cheng L., Bullock J. S., Gallazzi A., 2013, *ApJ*, 779, 102
- Lewis I. J., et al., 2002, *MNRAS*, 333, 279
- Lucchini S., D’Onghia E., Fox A. J., 2021, *ApJL*, 921, L36
- Mackey D., Koposov S. E., Da Costa G., Belokurov V., Erkal D., Kuzma P., 2018, *ApJ*, 858, L21
- Majewski S. R., Nidever D. L., Muñoz R. R., Patterson R. J., Kunkel W. E., Carlin J. L., 2008, *Proc. IAU*, 4, 51
- Massana P., et al., 2020, *MNRAS*, 498, 1034
- Nidever D. L., Monachesi A., Bell E. F., Majewski S. R., Muñoz R. R., Beaton R. L., 2013, *ApJ*, 779, 145
- Nidever D. L., et al., 2017, *MNRAS*, 154, 199
- Omkumar A. O., et al., 2020, *MNRAS*, 500, 2757
- Pardy S. A., D’Onghia E., Fox A. J., 2018, *ApJ*, 857, 101
- Pierres A., et al., 2017, *MNRAS*, 468, 1349
- Pietrzyński G., et al., 2019, *Nature*, 567, 200
- Schwarz G., 1978, *Ann. Statistics*, 6
- Scowcroft V., Freedman W. L., Madore B. F., Monson A., Persson S. E., Rich J., Seibert M., Rigby J. R., 2016, *ApJ*, 816, 49
- Sharp R., Birchall M. N., 2010, *PASA*, 27, 91
- Subramaniam S., et al., 2017, *MNRAS*, 467, 2980
- van der Marel R. P., Kallivayalil N., 2014, *ApJ*, 781, 121
- Zivick P., et al., 2018, *ApJ*, 864, 55
- Zivick P., Kallivayalil N., van der Marel R. P., 2021, *ApJ*, 910, 36

This paper has been typeset from a  $\text{\LaTeX}$  file prepared by the author.